JOC The Journal of Organic Chemistry

Article

pubs.acs.org/joc

1*H*-Azepine-2-oxo-5-amino-5-carboxylic Acid: A 3_{10} Helix Inducer and an Effective Tool for Functionalized Gold Nanoparticles

Sara Pellegrino,*[,†] Andrea Bonetti,[†] Francesca Clerici,[†] Alessandro Contini,[†] Alessandro Moretto,[§] Raffaella Soave,[‡] and Maria Luisa Gelmi[†]

[†]Dipartimento di Scienze Farmaceutiche- Sezione di Chimica Generale e Organica- "A. Marchesini" Università degli Studi di Milano, Via Venezian 21 20133, Milano, Italy

[§]Dipartimento di Scienze Chimiche, Università degli Studi di Padova, Via Marzolo 1 35131, Padova, Italy

[‡]CNR- Istituto di Scienze e Tecnologie Molecolari, Via Golgi 19 20133, Milano, Italy

Supporting Information

ABSTRACT: A new α,α-disubstituted constrained glutamine analogue has been designed to decorate gold nanoparticles and to induce a 3_{10}-helix when inserted in peptides. Using an efficient "one-pot" asymmetric Schmidt reaction between 4-disubstituted-cyclohexanone and hydroxyalkylazides, 1*H*-azepine-2-oxo-5-amino-5-carboxylic acid was prepared. The main (*R*) isomer was inserted at the N-terminus in a very short peptide sequence (i.e., PhCO-(*R*)-Oxo-Azn-L-Ala-Aib-L-AlaNHMe) and a stable 3_{10}-helix conformation was obtained, as verified by both NMR experiments and molecular dynamics (MD) simulations. Finally, the presence of the hydroxyl chain at the nitrogen atom of the ring allowed for the preparation of covered chiral gold nanoparticles.

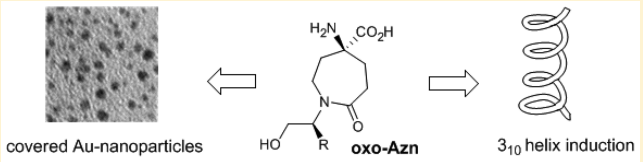

INTRODUCTION

Small molecule-functionalized gold nanoparticles (GNPs) are at the forefront of research in nanochemistry.[1] The three-dimensional self-assembled monolayers constructed by the introduction of organic compounds on GNPs have emerged as versatile tools for surface modification. Furthermore, the organic monolayer reduces the surface energy of GNPs and thus provides increased solubility and colloidal stability.[2]

Amino acids and peptides are effective building blocks for creating hierarchical nanomaterials[3] and functionalized GNPs.[4] They feature a multitude of functionalities and unique secondary structures based on controllable primary sequences and environmental conditions.[5] By using amino acids and peptides, it is thus possible to tailor new hybrid materials for a broad range of applications in different areas, such as medicine, bionanotechnology, and electrochemistry.[6] Conversely, focusing on biomedical applications, peptide instability toward proteases might be a concern. Synthetic analogues of natural amino acids represent valuable tools for overcoming this problem.[3b,7] In particular, the use of α,α-disubstituted derivatives gives the double advantage of reducing metabolic degradation and of stabilizing the helical conformation by reducing the available conformational space of the peptide backbone.[8]

Continuing our research on unnatural constrained amino acids,[9] we recently prepared an α,α-disubstituted ornithine analogue (i.e., 1*H*-azepine-4-amino-4-carboxylic acid, Azn) as an effective 3_{10}-helix inducer.[9c] With the aim of potentially using this scaffold as a key material for decorating gold nanoparticles, we designed an α,α-disubstituted cyclic glutamine analogue, 1*H*-azepine-2-oxo-5-amino-5-carboxylic acid (Oxo-Azn), containing a hydroxy tethering group on the nitrogen side chain (Figure 1).

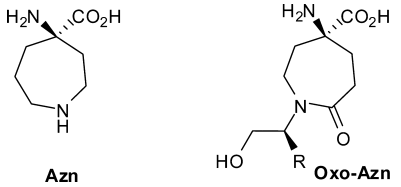

Figure 1. Chemical structures of Azn and Oxo-Azn.

Oxo-Azn was prepared using a very efficient one-step asymmetric Schmidt reaction that gives a mixture of "quasi enantiomers" that are easily separated by chromatography (Scheme 1). The main (*R*) isomer was thus inserted at the N-terminus in a very short peptide sequence (i.e., PhCO-(R)-Oxo-Azn-L-Ala-Aib-L-AlaNHMe). A stable 3_{10}-helix conformation was obtained and verified by both NMR experiments and molecular dynamics (MD) simulations. Finally, taking advantage of the tethering group, covered chiral gold nanoparticles were prepared and fully characterized.

RESULTS AND DISCUSSION

Synthesis of the Oxo-Azn Scaffold. 1*H*-Azepine-2-oxo-5-amino-5-carboxylic derivatives **5**/**6** were synthesized through an

Received: February 19, 2015
Published: May 4, 2015

DOI: 10.1021/acs.joc.5b00396
J. Org. Chem. 2015, 80, 5507−5516

Scheme 1. Asymmetric Schmidt Reaction on Ketone 1

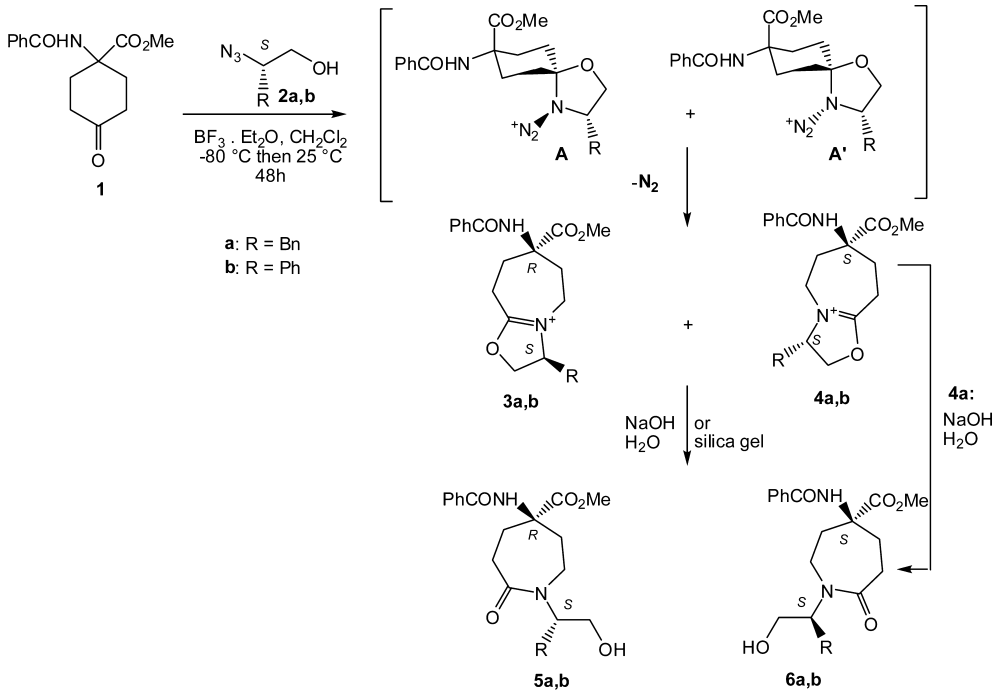

Scheme 2. Synthesis of Tetrapeptide PhCO-(*R*)-Oxo-Azn-L-Ala-Aib-L-AlaNHMe

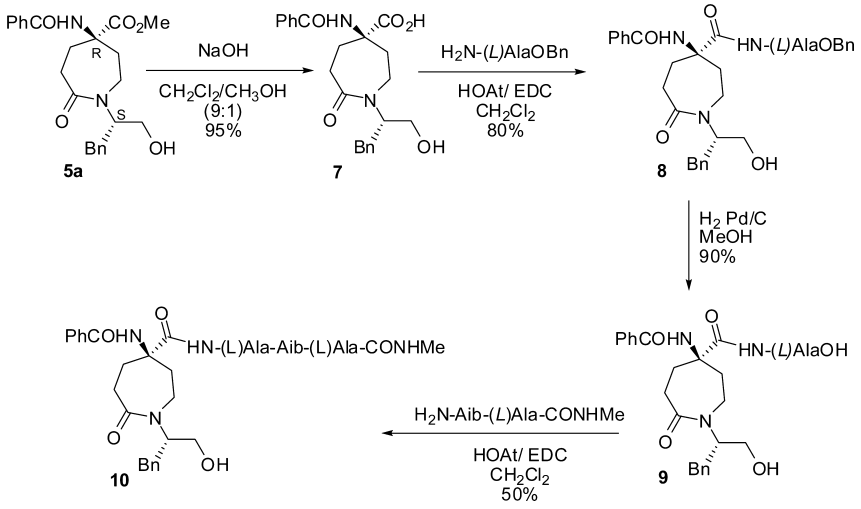

asymmetric Schmidt reaction[10] on cyclohexanone **1**[9c] and benzyl- or phenyl-substituted hydroxyalkylazides (**2a**,**b**) (Scheme 1). The reaction was performed in CH_2Cl_2 and in the presence of excess $BF_3{\cdot}OEt_2$ (−80 to 25 °C). After 48 h, the reaction was quenched with 2N NaOH, affording a mixture of "quasi enantiomers" **5** and **6** (67:33 **5a**/**6a**, 80%; 50:50 **5b**/**6b**, 75%; ^{1}H NMR and HPLC analyses). A similar diastereoselection and yield were obtained by changing the temperature (−10 to 25 °C) and reaction time (18 h).

To gain insight into the mechanism and diastereoselection, we monitored the reaction between **1** and **2a** by ^{1}H NMR. After 18 h, ^{1} H NMR analysis of the crude mixture, before NaOH quenching, showed the formation of intermediates **3a**/**4a** in a 67:33 ratio. This mixture was crystallized from Et_2O, affording pure bicyclic intermediate **4a** (13%). Pure azepinone derivatives **5a** (45%) and **6a** (10%) were isolated after column chromatography of the mother liquors (Scheme 2).

Finally, the treatment of **4a** with NaOH (2N, 24 °C, 30 min) gave minor stereoisomer **6a** in quantitative yield (Scheme 1). X-ray crystallography of single crystal of **4a** (Figure 2) allowed us to unequivocally assign the stereochemistry of each adduct (for NMR discussion, see the Supporting Information).

Isolation of rigid bicyclic intermediate **4a** allowed us to confirm that the mechanism of formation of "quasi enantiomers" **5**/**6** is the one proposed by Aubè et al.[10] Accordingly, the azido addition occurs on ketone **1**, which possesses the chair conformation bearing the amido group in the equatorial position (confirmed as the most stable by theoretical calculations). In this way, diastereoisomeric spiro intermediates **A** and **A**′, which differ in their stereochemistry of the nitrogen leaving group, are formed. Consequent to the departure of N_2, anti-periplanar migration of the methylene group of the cyclohexyl ring occurs, affording bicyclic salt **3** from **A** and salt **4** from **A**′ (Scheme 1).

DOI: 10.1021/acs.joc.5b00396
J. Org. Chem. 2015, 80, 5507−5516

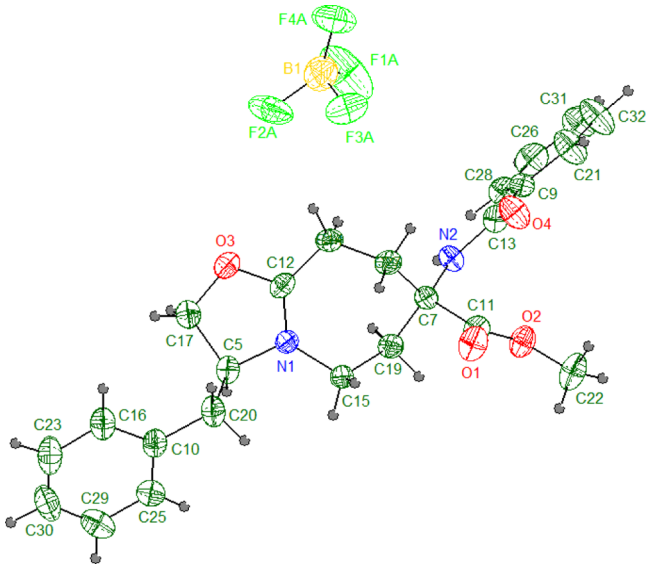

Figure 2. ORTEP plot of **4a** at 293 K with atom numbering scheme; ellipsoids of non-H atoms are at the 30% probability level.

Although the reaction occurred via the same mechanism, we found a different distribution of the diastereomers with respect to the literature data on 4-monosubstituted cyclohexanones. As an example,[10a] the Schmidt reaction between 4-*tert*-butylcyclohexanone and azide **2b** leads to *S* diastereoselection through the stabilization of intermediate **A**′ by cation-π interactions. In our case, using the same azide, no diastereoselection was observed, suggesting that steric factors drive the diastereoselection outcome. This hypothesis is confirmed by the partial diastereoselection found in the case of azide **2a** containing the more flexible benzyl substituent. In this case, minimization of steric interactions between the nitrogen leaving group and the benzyl substituent favors the formation of intermediate **3a** with respect to **4a**.

Synthesis of Tetrapeptide PhCO-(*R*)-Oxo-Azn-L-Ala-Aib-L-AlaNHMe. The model peptide PhCO-(*R*)-Oxo-Azn-L-Ala-Aib-L-AlaNHMe was then prepared starting from α,α-amino acid **5a** (Scheme 2). The sequence Ala-Aib-Ala has been deeply investigated in the literature using both experimental techniques (NMR, CD, X-ray) and MD.[11] In all of these studies, it has emerged that multiple conformations are present and that it is necessary to increase the length of the peptide chain to obtain stable helical conformations. Regarding Oxo-Azn, the *R*-isomer was selected because it is known that only the *R*-Azn isomer (see Figure 1) is able to induce a 3_{10}-helix when inserted in a short pentapeptide containing L-amino acids.[9c]

To acquire the necessary quantity of scaffold **5a** for the peptide synthesis optimization, the reaction between ketone **1** and azide **2a** was scaled up to 11 g of **1**, yielding **5a** in 47% yield after column chromatography purification. The ester function on scaffold **5a** was hydrolyzed using a methanolic solution of NaOH (2N) in CH_2Cl_2/MeOH (9:1, 25 °C, 15 h). Acid **7** was isolated in 95% yield. Compound **7** was made to react with alanine benzyl ester *p*-toluene sulfonate [HOAt (1 equiv)/EDC (1 equiv)/DIPEA (2 equiv), CH_2Cl_2, 25 °C, 2 h] to afford dipeptide **8** (58% yield). The yield of **8** was increased (80%) using the free amine derivative of alanine operating with the same condensative conditions (15 h). The benzyl group of the ester function was removed by hydrogenolysis (Pd/C, MeOH, 25 °C, 24 h) to give acid **9** (90%, Scheme 3). The final tetrapeptide (**10**, 50%) was obtained by the reaction of **9** with dipeptide H_2N-Aib-L-Ala-CONHMe [HOAt (1 equiv)/EDC (1 equiv)/DIPEA(2 equiv), CH_2Cl_2, 25 °C, 15 h]. It has to be noted that, in these reaction conditions, epimerization of the alanine stereocenter was not observed (HPLC analysis, Figure S4 in the Supporting Information). Any attempt to directly synthesize compound **10** from **5a** and H_2N-L-Ala-Aib-L-Ala-CONHMe tripeptide failed, probably because of the steric hindrance on the carboxylic function of **7**.

Tetrapeptide **10** was first purified by preparative reverse-phase HPLC. During the purification, we observed the formation of a byproduct corresponding to bicyclic derivative **11** (Figure 3, see the Supporting Information for NMR discussion). Its formation must be ascribed to the TFA present in the reverse-phase HPLC eluent phases that catalyzed the oxazoline ring formation. To overcome this issue, we directly purified compound **10** by crystallization (CH_2Cl_2/Et_2O) of the crude reaction mixture.

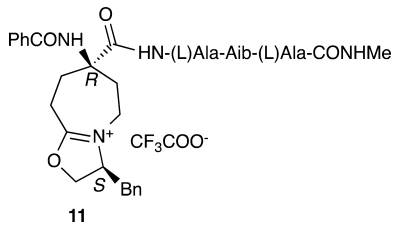

11

Figure 3. Chemical structure of **11**, the transformation product of **10**, in acidic conditions.

NMR Conformational Studies on Model Peptide 10. Full assignment of the protons of peptide **10** was accomplished by 500 MHz NMR analysis (1H, ^{13}C, COSY, TOXY, and HSQC NMR experiments; see the Supporting Information). 2D-NOESY at different mixing times and temperature-dependent chemical shift variation experiments (273−333 K) were performed in CD_3CN solution to obtain detailed information on the conformational behavior of **10**.

A complete set of N, N (i, i + 1) NOE cross-peaks [PhCONH/Ala-2 (w); Ala-2/Aib (m); Aib/Ala-4 (vs)] were

Scheme 3. Condensation between 5a and 3-Tritylsulfanyl Propionic Acid

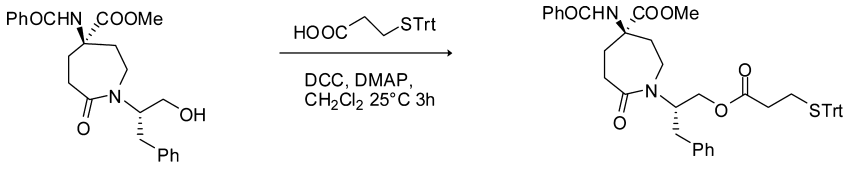

5a **12**

DOI: 10.1021/acs.joc.5b00396
J. Org. Chem. 2015, 80, 5507−5516

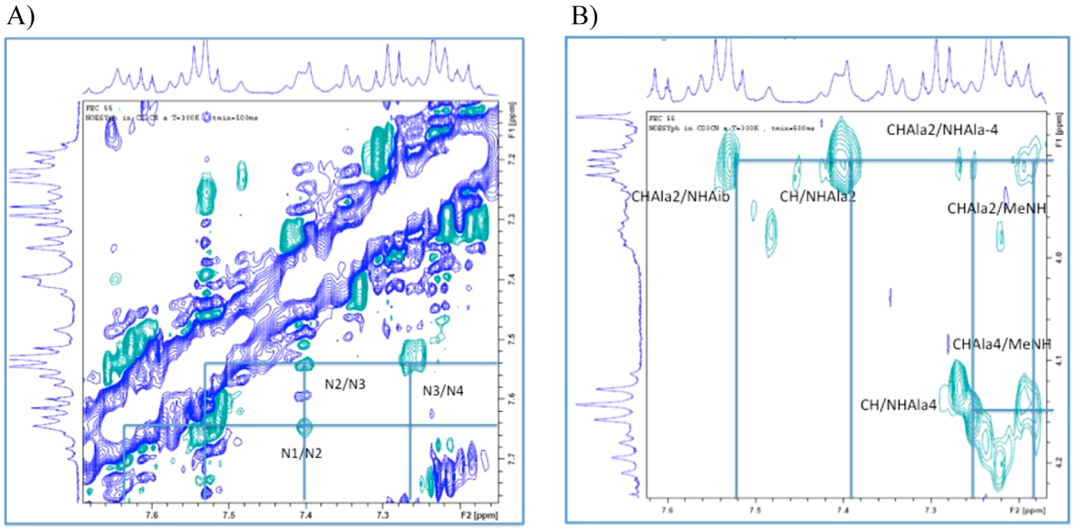

Figure 4. Sections of the NOESY spectrum of **10** (10.2 mM CD_3CN solution, 500 MHz, 25 °C, 500 ms mixing time) for (A) NH/NH and (B) α-H/NH NOE regions.

detected except for Ala-4/MeNH, which was overlapped (Figure 4A).

Various NOEs are operative in the peptide chain (i.e., α, N (i, i + 1) between Ala-2/Aib (m) and Ala-4/NHMe (w)) (Figure 4B). Longer range α, N (i, i + 2) and α, N (i, i + 4) NOEs allow for defining the helix types: the former is typical of a 3_{10}-helix, whereas the latter is typical of an α-helix.[9c] In our case, of relevance are the long-range NOEs of Ala-2/Ala-4 [α, N (i, i + 2; w) (Figure 4B), the phenyl ring of the benzyl moiety (δ 7.94), and the methyl of Aib (δ 1.54, m) (Figure 5). A further long-range NOESY was detected between Ala-2 and NHMe [α, N (i, i + 3; m)]. All of these data are in agreement with a 3_{10}-helix conformation.

^{13}C NMR values of the anisotropic Me of Aib that are in a magnetically inequivalent environment, such as in a helix structure, differ by more than 2 ppm.[11a] In our case, ^{13}C NMR δ values of 23.0 and 26.4 were found for the Aib Me groups. NH chemical shift temperature dependences, providing information on inaccessible or intramolecular H-bonds,[9c] also confirmed the helix structure. Values of −3.98 ppb K^{-1} for Oxo-Azn, −3.99 ppb K^{-1} for Ala-2, −2.57 ppb K^{-1} for Aib, −1.55 ppb K^{-1} for Ala-4, and −2.64 ppb K^{-1} for NHMe were detected (Figure 6).

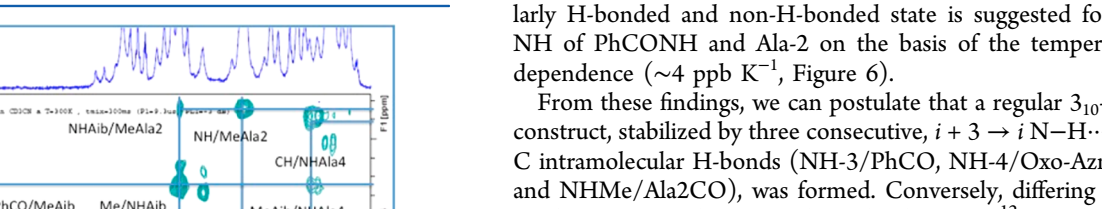

Figure 6. Temperature dependence of the NH proton chemical shifts of compound **10**.

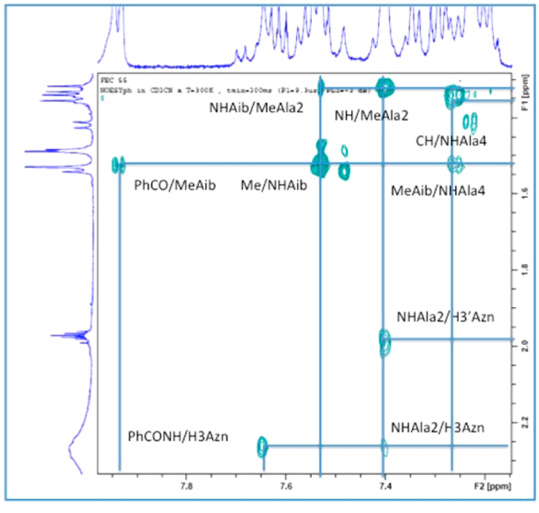

Figure 5. Section of the NOESY spectrum of **10** (10.2 mM CD_3CN solution, 500 MHz, 25 °C, 300 ms mixing time) for the NH/β-H NOE region.

These data suggest that NH of Aib, Ala-4, and NHMe fall within the typical ranges for intramolecularly H-bonded protons. Conversely, an equilibrium between an intramolecularly H-bonded and non-H-bonded state is suggested for the NH of PhCONH and Ala-2 on the basis of the temperature dependence (~4 ppb K^{-1}, Figure 6).

From these findings, we can postulate that a regular 3_{10}-helix construct, stabilized by three consecutive, i + 3 → i N−H···O═C intramolecular H-bonds (NH-3/PhCO, NH-4/Oxo-AznCO, and NHMe/Ala2CO), was formed. Conversely, differing from similar compounds reported in the literature,[12] we did not detect any intramolecular H-bonds between the CO group of the lactame function and the NH of the peptide chain that could compete in the helix formation. Therefore, the ability of Oxo-Azn to strongly stabilize 3_{10}-helix even with very short peptides has to be stressed.

Molecular Dynamics (MD) Studies on Model Peptide 10. To evaluate the folding behavior of (*R*)-Oxo-Azn, we also performed replica exchange molecular dynamics (REMD) simulations starting from a fully extended conformation of peptide **10** (φ = ψ = ω = 180°) according to the protocol reported in our previous studies.[8a,9c,h] The resulting trajectory, extracted from each replica to simulate a constant temperature of 308.5 K, was then analyzed in terms of H-bonds, secondary structure, and cluster analyses (Tables 1−3, Figure 7).

DOI: 10.1021/acs.joc.5b00396
J. Org. Chem. 2015, 80, 5507−5516

Table 1. Results of DSSP Analysis of the 100 ns REMD Trajectory Obtained at T = 308.53 K[a]

residue	3_{10}-helix	α-helix	turn
Oxo-Azn1	31.1	3.6	19.7
Ala2	34.7	3.6	25.8
Aib3	34.7	3.6	31.5
Ala4	18.7	3.6	30.0

[a]Values are reported as a percentage of the total secondary structure populations. The difference to 100% is the percentage of unordered secondary structure.

Table 2. Results of H-Bond Analysis of the 50−100 ns REMD Trajectory at T = 308.53 K

acceptor	donor	occ. (%)	av dist.[a] (Å)	av angle[b] (deg)
Ph C═O	Aib3 NH	37.0	3.20	163.1
Ala2 C═O	NHMe	27.0	3.13	160.5
Oxo-Azn1 C═O	Ala4 NH	19.1	3.32	162.0
Oxo-Azn1 C═O	NHMe	5.3	3.13	161.9
Ph C═O	Ala4 NH	3.9	3.42	162.9

[a]Donor−acceptor distance; cutoff = 4.0 Å. [b]Donor−H-acceptor angle; cutoff = 150 deg.

The results show that Oxo-Azn has a helical propensity similar to that observed for the parent Azn,[8a,9c] suggesting that neither the lactame C═O nor the substituted chain at the nitrogen azepino negatively affect the ability to stabilize helical conformations. Indeed, the DSSP analysis of the REMD 308.53 K (Table1) trajectory shows a relatively high helical content for residues 1−3 with turn content prevalent only for the C-terminal residue Ala4. It can also be observed that the helical content is principally due to a 3_{10}-helix conformation with only a marginal contribution of α-helix. This is also confirmed by H-bond analysis (Table 2), because relevant H-bonds are those of the $i \rightarrow i + 3$ type (Ph C═O···HN Aib3, Oxo-Azn C═O···HN Ala4, and Ala2 C═O···HNMe) typical of 3_{10} helices, whereas $i \rightarrow i + 4$ H-bonds show occupancies of ∼5%. Finally, geometrical clusterization (Figure 8) followed by the analysis of relevant φ and ψ dihedrals (Table 3) showed a helical conformation as the well-defined secondary structure most frequently sampled during the simulation (cluster #1, pop % = 41.3, Figure 7), even if structures classifiable as different folding intermediates (clusters #2−5) represent ∼60% of the whole conformational population. By observing the average φ and ψ values of the most populated cluster (#1), it can be observed that most dihedrals fall within the range typical of a 3_{10} helix (even if an α-helix cannot be excluded, if deviations from the average values are considered).[13] Further details on the folding preferences of peptide **10** were also provided by analysis of the

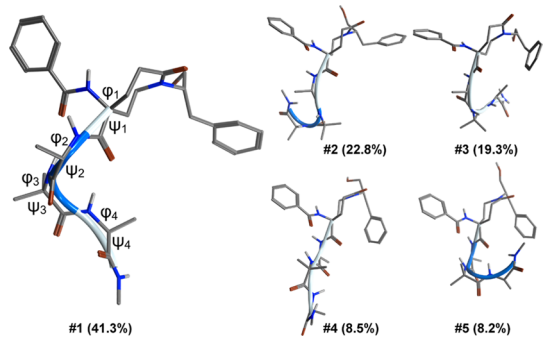

Figure 7. Representative structure and relative population (%) of the most populated clusters obtained by cluster analysis of the 50−100 ns REMD trajectory obtained at T = 308.53 K.

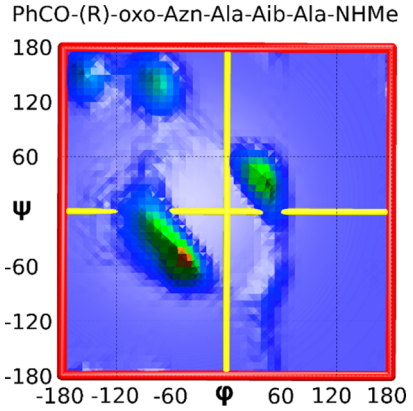

Figure 8. 3D Ramachandran plot obtained from the 100 ns REMD trajectory (308.53 K) of peptide **10**. The z-axis represents the frequency of occurrence.

three-dimensional (3D) Ramachandran plot derived from the 100 ns REMD trajectory obtained at 308.53 K (Figure 8).

It can be observed that the most frequently sampled couple of φ and ψ dihedrals is that typical of the right-handed helix secondary structure, followed by a non-negligible amount of left-handed helix. Dihedral values belonging to the β regions are also sampled and, interestingly, the paths connecting the different regions of the 3D Ramachandran plot can also be observed as ruffles on the graph surface, which indicate high energy conformations that are only occasionally sampled.

Use of Scaffold 5 for Gold Nanoparticle Preparation. Finally, we investigated the possibility of using scaffold **5** for obtaining covered gold nanoparticles. First, we introduced a thiol tether through an ester linkage with the hydroxy function of scaffold **5**. 3-Tritylsulfanyl propionic acid was condensed

Table 3. Average Dihedrals Obtained from Analysis of the Three Most Populated Cluster Trajectories

	#1	#2	#3	#4	#5
φ1	−29 ± 35	15 ± 43	22 ± 41	−16 ± 43	33 ± 29
ψ1	−33 ± 35	18 ± 47	23 ± 47	−20 ± 43	35 ± 32
φ2	−60 ± 26	−87 ± 48	−93 ± 40	−64 ± 41	35 ± 44
ψ2	−22 ± 19	111 ± 81	132 ± 69	4 ± 46	32 ± 17
φ3	−45 ± 13	−22 ± 38	40 ± 19	22 ± 38	46 ± 9
ψ3	−44 ± 29	−24 ± 55	27 ± 63	7 ± 72	43 ± 16
φ4	−85 ± 27	−87 ± 35	−75 ± 60	−87 ± 44	−78 ± 55
ψ4	16 ± 65	49. ± 81	87 ± 86	80 ± 91	70 ± 92

DOI: 10.1021/acs.joc.5b00396
J. Org. Chem. 2015, 80, 5507−5516

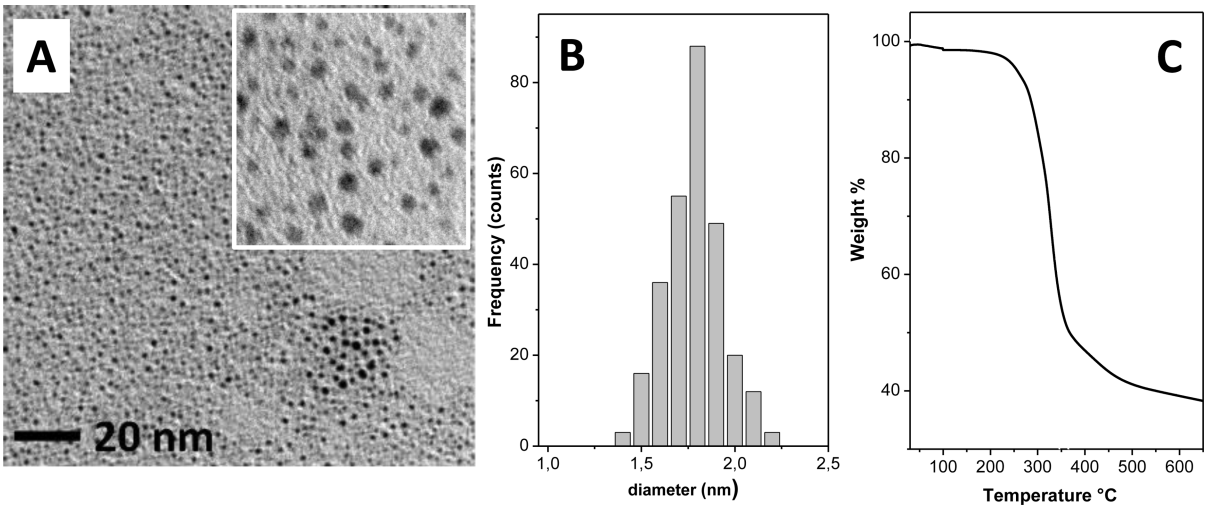

Figure 9. (A) TEM image showing the formation of AuNp-**12** conjugates. Inset, detailed view of the AuNp-**12** conjugates. (B) AuNp-**12** conjugated size distribution graph showing an average diameter of 1.8 nm. (C) TGA analysis of AuNp-**12** conjugates showing a 55% weight loss referring to the organic part of the cluster.

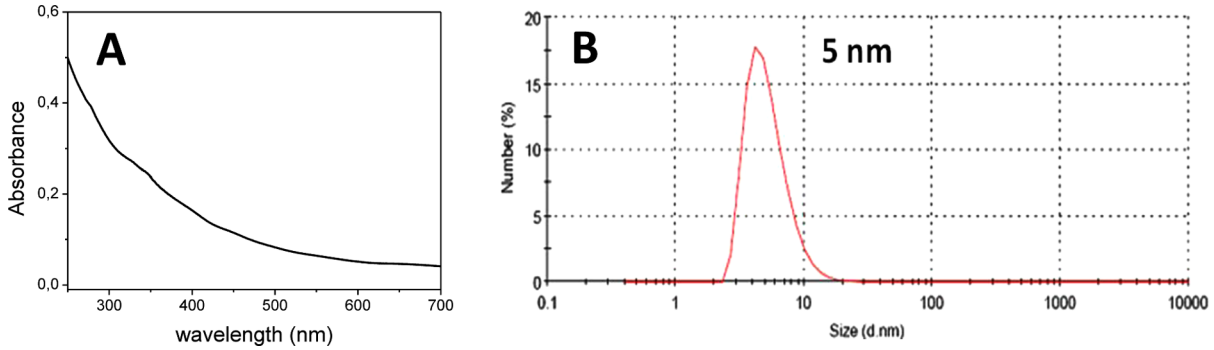

Figure 10. (A) UV−vis absorption spectra in CH_2Cl_2 solution of AuNp-**12** conjugates. (B) DLS distribution of AuNp-**12** conjugates recorded in a CH_2Cl_2 solution.

with scaffold **5** using DCC and DMAP (CH_2Cl_2, 25 °C, 3 h) affording compound **12** (80%, Scheme 3).

Gold nanoparticles (AuNp) were prepared by chemical reduction (with $NaBH_4$) in a methanol/water mixture of the corresponding tetrachlorohydrate salts in the presence of amino acid conjugate **12**.[6b] The resulting dark-brown nanoparticle conjugates were found to be soluble in organic solvents, such as CH_2Cl_2 and $CHCl_3$. Transmission electron microscopy analysis (TEM) revealed the formation of AuNp-**12** conjugated with a metallic core average diameter of 1.8 nm (Figure 9A and B). Moreover, thermogravimetric analysis (TGA) showed a 55% weight loss, which is to attributed to the organic part of the cluster, thus confirming the effective incorporation of **12** over the nanoparticle surface (Figure 9C).

Furthermore, UV−vis absorption spectra and dynamic light scattering (DLS), both recorded in CH_2Cl_2 solution, supported the formation of such nanoparticles (Figure 10A and B, respectively). In particular, UV−vis absorption spectra showed a continuous absorption profile in the 300−700 absorption region, and this finding is typical for gold nanoparticles with a diameter size below 2 nm.[14] DLS analysis revealed a 5 nm particle size distribution, which is in accordance with the bulky nature of the ligand. Moreover, IR (KBr) analysis showed typical amide bond signals [ν: 3297 (NH-amides), 1734 (CO esters), 1651 (CO amide I), 1546 (CO amide II) cm^{-1}] that confirmed the occurrence of AuNp-**12** conjugation by showing the preservation of the functional groups of **5a** after it links to the gold core.

Interestingly, AuNp-**12** presents a dichroic spectrum in the 350−680 nm region (Figure 11), which can be attributed to the

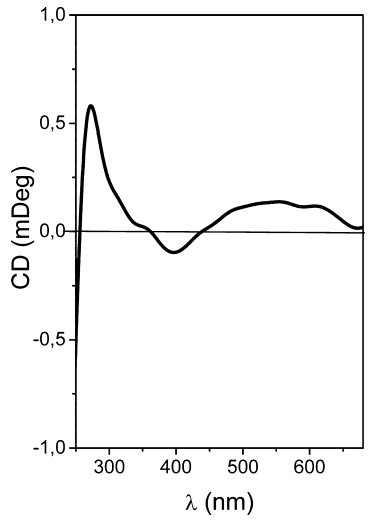

Figure 11. CD spectrum of AuNp-**12** in dioxane at 20 °C in the 250−680 nm region.

DOI: 10.1021/acs.joc.5b00396
J. Org. Chem. 2015, 80, 5507−5516

gold core. In particular, the CD spectrum of AuNp-**12** showed two positive bands located at 300 (intense) and 500 (broad) nm, whereas a weak negative band was displayed at 400 nm. Similar findings were reported in the literature and attributed to metal-chiral ligand interactions[15] that enhanced the intrinsic chirality of the Au core.[16]

Finally, by combining the information from TEM and TGA analyses, we propose a structure of AuNp-**12** conjugates that results in a chemical formula of $Au_{201}L_{60}$.

In conclusion, the new glutamine analogue Oxo-Azn functionalized on the nitrogen side chain with a hydroxyalkyl tether was efficiently synthesized in the enantiopure form and on the gram scale by an asymmetric one-step procedure. Both theoretical and dynamic NMR studies revealed that *R*-Oxo-Azn is a good 3_{10}-helix inducer when inserted at the N-terminus in a short peptide sequence. Finally, the presence of the tethering group allowed for the preparation of covered chiral gold nanoparticles. Considering the helical stabilization of Oxo-Azn in solution described above, it will be worthwhile in the future to deeply investigate if this ability is also maintained when linked to gold nanoparticles.

EXPERIMENTAL SECTION

The materials and solvents were purchased from common commercial sources and used without additional purification. ^{1}H NMR spectra were recorded at 200, 400, or 500 MHz and ^{13}C NMR spectra at 50, 70, or 125 MHz using TMS as an internal standard. The following abbreviations were used to describe peak patterns where appropriate: singlet (s), doublet (d), triplet (t), multiplet (m), and broad resonances (br). Coupling constants (*J*) are reported in hertz. Mass spectra were recorded under electron spray interface (ESI) conditions. Infrared spectra were recorded on an FTIR spectrometer. Values of $[\alpha]_D$ were measured using $CHCl_3$ as the solvent, if not explicitly reported. UV−vis absorption spectra were measured in water on a UV−vis spectrophotometer with 1 cm path length quartz cuvettes. Samples for transmission electron microscopy (TEM) were prepared before use by 100-fold dilution of a 2 mg/mL water solution of the AuNp. A glow discharged carbon-coated grid was floated on a small drop of solution and excess was removed by #50 hardened filter paper. Thermogravimetric analysis (TGA) was run on 5 mg nanoparticle samples from 25 to 1200 °C under a continuous N_2 flow.

Theoretical Calculations. The charge parametrization of the unnatural Oxo-Azn amino acid has been performed as previously reported.[8a,9c] Briefly, the Oxo-Azn structure was designed with MOE,[17] capped with acetyl (Ac) and NHMe groups at the N- and C-termini, respectively, and submitted to a conformational search with MOE using the following setup: Low Mode MD, MMFF94x force field, Born solvation, iteration limit = 40000, MM iteration limit = 2500, and rejection limit = 500. The two lowest energy conformations having φ and ψ dihedrals matching a right- and left-handed helix (φ = ± 60°, ψ = ± 45°) were selected for charge parametrization with R.E.D.IV.[18] The geometries were than optimized at the HF/6-31G(d) level and two different spatial orientations were used to derive RESP-A1 charges. Charge restraints of −0.4157, 0.2719, 0.5973, and −0.5679 were imposed to the backbone nitrogen, hydrogen, carbonyl carbon, and oxygen, respectively, according to the Amber ff99SB force field.[19]

REMD simulations were carried out on model peptide **10** starting from an extended conformation ($\psi = \varphi = \omega = 180°$) and by following a previously reported protocol,[8a,9c] Briefly, 12 replicas were run for 100 ns at temperatures from 260.00 to 658.94 K, using the pmemd module of Amber14[20] and selecting the ff99SB force field coupled with the GB-OBC(II) implicit solvent model.[21] The trajectories were extracted at 308.53 K, and the simulation convergence was assessed on the basis of cluster analyses performed with cpptraj[20]at 25−50, 50−75, and 75−100 ns time intervals. The simulations were already fully converged at 50 ns, and the subsequent H-bond and clustering analyses were then conducted on the 50−100 ns interval. H-bonds were analyzed with VMD 1.9.1[22] with a donor−acceptor distance threshold of 4.0 Å and an angle cutoff of 30°. Secondary structure analyses were performed on the whole trajectory using the DSSP method[23] as implemented in cpptraj.

General Procedure for the Schmidt Reaction. Method A: Ketone **1**[9c] (11 g, 40 mmol) was dissolved in dry CH_2Cl_2 (300 mL) under nitrogen atmosphere. After cooling at −10 °C, $BF_3(OEt)_2$ (26.5 mL, 200 mmol) was added dropwise, and the mixture was incubated for 30 min after which azide **2a** or **2b** (1.3 equiv) dissolved in CH_2Cl_2 (200 mL) was added. Stirring was continued (TLC: CH_2Cl_2/MeOH, 10:1), and the temperature was gradually increased to 25 °C in over an 18 h period. A solution of NaOH (2N, until pH 14) was added, and the mixture was stirred for 30 min. A white solid, corresponding to isomer **6**, was formed and filtered. The organic layer was separated, and the aqueous layer was extracted with CH_2Cl_2 (3 × 50 mL). The organic layers were washed with a saturated solution of NH_4Cl (pH 4). After drying over Na_2SO_4 and solvent evaporation, the crude mixture was purified by chromatography on silica gel to afford diastereoisomers **5** and **6**.

Method B: The reaction of azide **2a** (275 mg, 1.3 mmol) and ketone **1** (300 mg, 1.1 mmol) was performed according to method A but without quenching by NaOH. After solvent evaporation, ^{1}H NMR analysis of the crude mixture showed the formation of a mixture of **3a**/**4a** in a 67:33 ratio. The reaction mixture was taken up with Et_2O, affording pure compound **4a** (60 mg, 13%), that was collected by filtration. The mother liquors were purified by chromatography (CH_2Cl_2/MeOH, from 100:0 to 50:1) to afford **5a** (210 mg, 45%) and **6a** (50 mg, 10%).

Methyl 5-Benzoylamino-1-[(*S*)-1-hydroxy-3-phenylpropan-2-yl]-2-oxoazepan-5-carboxylate (67:33 5a/6a). Column chromatoghraphy conditions: CH_2Cl_2/MeOH, from 100:0 to 10:1.

(*R*)-**5a**: 8.5 g, 47%; mp 234 °C (CH_2Cl_2/MeOH); $[\alpha]_D^{25}$ −24.7 (*c* 0.2, DMSO); IR (KBr) ν_{max} 3340, 1723, 1660 cm^{-1}; ^{1}H NMR (DMSO-d_6, 500 MHz) δ 8.55 (s, 1H, exch), 7.84 (d, *J* = 7.1, 2H), 7.57−7.18 (m, 8H), 4.77 (t, *J* = 5.3, 1H, exch.), 4.74 (brs, 1H), 3.56 (s, 3H, OMe), 3.54−3.48 (m, 2H), 3.45−3.39 (m, 1H), 3.35−3.27 (m, 1H), 2.86 (dd, *J* = 15.2, 6.3, 1H), 2.75 (dd, *J* = 15.2, 9.5,1H), 2.65−2.55 (m, 1H), 2.30−2.18 (m, 2H), 2.14−2.05 (m, 1H), 1.85−1.68 (m, 2H); ^{13}C NMR (DMSO-d_6, 125 MHz) δ 28.2, 31.3, 34.1, 34.6, 38.2, 51.7, 55.8, 59.9, 60.9, 125.7, 127.5 (x2), 127.9 (x4), 128.4 (x2), 131.2, 133.8, 138.6, 166.6, 173.4, 173.9; MS (ESI+) 447.3 [M + 23] $C_{24}H_{28}N_2O_5$ Calcd for C 67.91, H 6.65, N 6.60; found C 67.78, H 6.80, N 6.49.

(*S*)-**6a**: 4.1 g, 23%; mp 230 °C dec (CH_2Cl_2/*n*-hexane); $[\alpha]_D^{25}$ −47.7 (*c* 0.1, DMSO); IR (KBr) ν_{max} 3435, 1737, 1627 cm^{-1}; ^{1}H NMR (DMSO-d_6, 500 Mz) δ 8.51 (s, 1H, exch), 7.82 (d, *J* = 7.1, 2H), 7.58−7.15 (m, 8H), 4.75 (t, *J* = 4.8, 1H, exch.), 4.54 (brs, 1H), 3.58 (s, 3H), 3.55−3.42 (m, 3H), 3.35−3.22 (m, 1H), 2.24−2.71 (m, 2H), 2.66 (dd, *J* = 13.1, 13.6, 1H), 2.38−2.28 (m, 1H), 2.25−2.07 (m, 2H), 1.83 (dd, *J* = 13.5, 12.8, 1H), 1.81−1.70 (brs, 1H); ^{13}C NMR (DMSO-d_6, 125 Mz) δ 28.2, 31.2, 34.1, 34.3, 39.1, 51.7, 57.8, 60.1, 60.9, 125.7, 127.5 (x2), 127.9 (x2), 127.9 (x2), 128.6 (x2), 131.2, 133.9, 138.8, 166.9, 173.6, 173.9; MS (ESI+) 447.2 [M + 23]; $C_{24}H_{28}N_2O_5$ Calcd for C 67.91, H 6.65, N 6.60; found C 67.78, H 6.80, N 6.49.

Methyl 5-Benzoylamino-1-[(*S*)-2-hydroxy-1-phenylethyl]-2-oxoazepan-5-carboxylate (50:50 5b/6b). Column chromatoghraphy conditions: CH_2Cl_2/MeOH, from 100:0 to 50:1

(*R*)-**5b**: 5.7 g, 35%; mp 260 °C (CH_2Cl_2/MeOH); $[\alpha]_D^{25}$ +13.2 (*c* 0.2, MeOH); IR (KBr) ν_{max} 3359, 1726, 1624 cm^{-1}; ^{1}H NMR (DMSO-d_6, 300 MHz) δ 8.58 (s, 1H, exch), 7.84 (d, *J* = 8.2, 2H), 7.58−7.25 (m, 8H), 5.63 (t, *J* = 6.8, 1H), 4.93 (brs, 1H, exch), 3.88 (t, *J* = 4.7, 2H), 3.54 (s, 3H), 3.56−3.54, 3.30−3.20 (2 m, 2H), 2.74 (dd, *J* = 2.5, 2.0, 1H), 2.55−2.25 (m, 2H), 2.10−1.85 (m, 2H), 1.50 (br, 1H); ^{13}C NMR (DMSO-d_6, 75 Mz) δ 29.6, 32.3, 35.5, 39.3, 52.8, 58.0, 60.6, 61.0, 128.1, 128.6 (x2), 128.7 (x2), 129.0 (x2), 129.2 (x2), 132.3, 134.9, 139.5, 167.7, 174.5, 174.9; MS (ESI+) 411.2 [M + 1], 433.3 [M + 23]; $C_{23}H_{26}N_2O_5$ Calcd for C 67.30, H 6.38, N 6.82; found C 67.01, H 6.55, N 6.63.

DOI: 10.1021/acs.joc.5b00396
J. Org. Chem. 2015, 80, 5507−5516

(*S*)-**6b** (trace amount of **5b** is present): 4.9 g, 30%; IR (KBr) ν_{max} 3412, 1738, 1627 cm^{-1}; ^1H NMR (DMSO-d_6, 300 MHz) δ 8.49 (s, 1H, exch), 7.85 (d, J = 7.2, 2H.), 7.56−7.20 (m, 8H.), 5.66 (dd, J = 13.8, 5.9, 1H), 4.93 (t, J = 4.8, 1H, exch), 4.00−3.75 (m, 2H), 3.60 (s, 3H), 3.53 (dd, J = 15.9, 10.1, 1H), 3.13 (dd, J = 15.9, 6.1, 1H), 2.89 (t, J = 13.5, 1H), 2.60−2.40 (m, 1H), 2.28 (dd, J = 14.5, 8.3, 1H), 2.25−2.10 (m, 1H), 2.10−1.85 (m, 2H); ^{13}C NMR (DMSO-d_6, 75 MHz) δ 29.1, 32.1, 35.8, 39.4, 52.9, 57.9, 60.5, 61.3, 127.9, 128.4 (x2), 128.7 (x2), 129.0 (x2), 129.2 (x2), 132.2, 135.0, 139.7, 167.9, 174.8, 175.5; MS (ESI+) 411.4 [M + 1], 433.4 [M + 23]; $C_{23}H_{26}N_2O_5$ Calcd for C 67.30, H 6.38, N 6.82; found C 66.97, H 6.54, N 6.58.

Methyl 7-Benzoylamino-(*S*)-3-benzyl-3,5,6,7,8,9-hexahydro-oxazolo[3,2-*a*]azepinium-7-carboxylate·BF_4^- (67:33 3a/4a). (*R*)-**3a** (mixture with (*S*)-**4a**): ^1H NMR ($CDCl_3$, 500 MHz, main signals) δ 7.92 (d, J = 7.1, 2H), 4.91 (m, 1H), 4.70 (m, 1H), 4.68 (m, 1H), 4.10−4.00 (m, 1H), 3.69 (s, 3H, OMe), 2.00−1.70 (m, 2H); ^{13}C NMR ($CDCl_3$, 125 MHz) δ 23.1, 27.7, 29.7, 32.1, 36.7, 42.5, 53.1, 60.2, 65.6, 76.3, 127.6 (x2), 127.9, 128.6 (x2), 129.2 (x2), 129.4 (x2), 132.2, 132.8, 133.5, 167.9, 173.1, 179.0.

(*S*)-**4a**: IR (KBr) ν_{max} 3400, 1738, 1661 cm^{-1}; ^1H NMR ($CDCl_3$, 500 MHz) δ 7.88 (d, J = 7.2, 2H), 7.50−7.46 (m, 1H), 7.42−7.37 (m, 5H), 7.36−7.33 (m, 1H), 7.22 (d, J = 6.9, 2H), 5.03 (dd, J = 9.8, 9.3, 1H), 4.97−4.90 (m, 1H), 4.68 (dd, J = 9.3, 5.9, 1H), 3.98 (dd, J = 15.1, 8.5, 1H), 3.81 (dd, J = 15.1, 9.3, 1H), 3.74 (s, 3H), 3.25 (dd, J =14.4, 5.0, 1H), 3.09 (dd, J = 17.7, 10.3, 1H), 3.04 (dd, J = 14.4, 7.5, 1H), 2.86 (dd, J = 17.7, 8.8, 1H), 2.82 (dd, J = 16.7, 9.2, 1H), 2.67 (ddd, J = 16.3, 9.0, 1.6, 1H), 2.30−2.59 (dd, J = 15.6, 8.3 1H), 2.54 (ddd, J = 16.3, 13.5, 1.8, 1H); ^{13}C NMR ($CDCl_3$, 125 MHz) δ 21.9, 26.4, 31.4, 36.3, 41.8, 52.3, 59.2, 64.6, 75.5, 126.8 (x2), 127.5, 127.9 (x2), 128.5 (x2), 128.8 (x2), 131.4, 132.1, 132.2, 166.9, 172.2, 178.6; MS (ESI+) 407.3 $[M]^+$; $C_{24}H_{27}N_2O_4$. Calcd for: C 70.74, H 6.68, N 6.87; found: C 70.62, H 6.90, N 6.68.

(*R*)-5-Benzoylamino-1-[(*S*)-1-hydroxy-3-phenylpropan-2-yl]-2-oxoazepane-5-carboxylic acid (7). Ester **5a** (300 mg, 0.7 mmol) was dissolved in CH_2Cl_2/MeOH (9:1, 10.5 mL). A methanolic solution of NaOH (2N, 1.13 mL) was added, and the mixture was stirred at 25 °C for 15 h (TLC: CH_2Cl_2/MeOH, 10:1). After solvent evaporation, the mixture was taken up with H_2O and acidified to 12N with HCl until pH 1. A solid was separated and filtered corresponding to acid **7** (220 mg). The aqueous solution was extracted with CH_2Cl_2 (3 × 3 mL). The organic layers were then dried over Na_2SO_4, and the solvent was removed under vacuum. After crystallization, a further crop of pure compound **7** was obtained (50 mg). Acid **7** (270 mg) was obtained in 95% overall yield.

Mp 180 °C (Et_2O); $[\alpha_D]^{25}$ +18.3 (c 0.1, MeOH); IR (KBr) ν_{max} 3353, 2923, 1720 cm^{-1}; ^1H NMR (DMSO-d_6, 300 MHz) δ 12.28 (brs, 1H), δ 8.40 (s, 1H), 7.84 (d, J = 7, 2H), 7.59−7.17 (m, 8H), 4.93−4.71 (m, 1H), 4.30 (brs, 1H), 3.65−3.27 (m, 4H), 2.97−2.70 (m, 2H), 2.63−2.42 (m, 1H), 2.38−2.01 (m, 3H), 1.98−1.80 (m, 2H); ^{13}C NMR (DMSO-d_6, 75 MHz) δ 29.3, 32.5, 35.2, 35.8, 42.1, 57.2, 61.9, 65.4, 126.8, 128.5 (x2), 128.9 (x 2), 129.0 (x2), 129.5 (x2), 132.1, 135.2, 139.7, 162.3, 175.1, 175.4; MS (ESI−) 409.6 [M − 1]; $C_{23}H_{26}N_2O_5$ Calcd for C 67.30, H 6.38, N 6.82; found C 67.13, H 6.53, N 7.01.

Synthesis of Dipeptide 8. Benzyl ester of (*L*)-alanine *p*-toluenesulfonate (200 mg, 1.11 mmol) was suspended in CH_2Cl_2 (5 mL) and then treated with triethylamine (155 μL, 1.11 mmol). The mixture was washed with H_2O. The organic layer was dried over Na_2SO_4, and the solvent was evaporated under vacuum. Acid **7** (130 mg, 0.320 mmol) was dissolved in a mixture of CH_2Cl_2 (3.2 mL) and DMF (0.1 mL). After cooling to 0 °C, HOAt (44 mg, 0.320 mmol), EDC (61 mg, 0.320 mmol), alanine benzyl ester (170 mg, 0.950 mmol), and DIPEA (2 equiv, 0.112 mL, until pH 8) were added to the mixture. The reaction was stirred overnight at 25 °C (TLC: CH_2Cl_2/MeOH, 10:1). The crude product was washed with aqueous HCl (3N, 2 × 5 mL), H_2O (5 mL), and finally with $NaHCO_3$ (2 × 5 mL). The organic layer was dried over Na_2SO_4, and the solvent was evaporated under vacuum. The crude mixture was crystallized to afford pure compound **13** (185 mg, 80%). Mp 120 °C (CH_2Cl_2/Et_2O); $[\alpha_D]^{25}$ −27.5 (c 0.1, MeOH); IR (KBr) ν_{max} 3400, 1740 cm^{-1}; ^1H NMR ($CDCl_3$, 300 MHz) δ 7.77 (d, J = 6.9, 2H), 7.48−7.14 (m, 14 H), 7.01 (s, 1H), 5.11 (q, J = 11.9, 2H), 4.70 (brs, 1H), 4.53 (t, J = 14.07, 1H), 3.72−3.57 (m, 2H), 3.46−3.26 (m, 2H), 2.85−2.52 (m, 4H), 2.29−2.02 (m, 4H), 1.38−1.27 (m, 3H), 1.27 (s, 1H); ^{13}C NMR ($CDCl_3$, 75 MHz) δ 18.3, 29.3, 32.3, 35.2, 36.1, 40.9, 48.8, 59.5, 61.6, 63.1, 67.4, 127.0, 127.2, 127.4, 127.7, 128.4, 128.5 (x2), 128.6, 128.7, 128.9, 129.0, 129.1, 129.3, 129.8, 132.3, 134.4, 135.7, 138.2, 168.4, 172.9, 173.1, 176.4; MS (ESI−) 570.9 [M − 1]; $C_{33}H_{37}N_3O_6$ Calcd for C 69.33, H 6.52, N 7.35; found C 69.57, H 6.23, N 7.04.

Debenzylation of Ester 8. Ester **8** (100 mg, 0.175 mmol) was dissolved in MeOH (5 mL). Pd/C (185 mg, 0.175 mmol) was added, and the mixture was hydrogenated at 25 °C overnight (TLC: CH_2Cl_2/MeOH, 10:1). The catalyst was filtered on a Celite pad, and acid **9** (75 mg, 90%) was obtained after crystallization. Mp 140 °C (CH_2Cl_2/Et_2O); $[\alpha_D]^{25}$ −20.8 (c 0.2, MeOH); IR (KBr) ν_{max} 3400, 2928, 1730, 1629 cm^{-1}; ^1H NMR (CD_3OD, 300 MHz) δ 7.85−7.82 (m, 2H), 7.57−7.43 (m, 3H), 7.31−7.19 (m, 5H), 4.32 (q, J = 7.1, 1H), 3.76−3.63 (m, 2H), 3.55 (brs, 2H), 3.36−3.31 (m, 2H), 2.92−2.78 (m, 2H), 2.61−2.41 (m, 3H), 2.23−2.01 (m, 3H), 1.35 (d, J = 7.1, 3H); ^{13}C NMR (CD_3OD, 75 MHz) δ 17.2, 28.3, 31.8, 34.8, 35.6, 39.8, 48.6, 49.2, 58.6, 61.6, 126.5, 127.5, 127.6, 127.7, 128.5 (x2), 128.8 (x2), 129.1, 131.8, 134.8, 138.5, 169.5, 174.1, 175.8, 176.8; MS (ESI+) 504.3 [M + 23]; $C_{26}H_{31}N_3O_6$ Calcd for C 64.85, H 6.49, N 8.73; found C 64.56, H 6.78, N 8.46.

Synthesis of Tetrapeptide 10. Acid **9** (60 mg, 0.125 mmol) was suspended in a mixture of CH_2Cl_2 (1.25 mL) and DMF (0.1 mL). After cooling to 0 °C, HOAt (17 mg, 0.125 mmol), EDC (24 mg, 0.125 mmol), dipeptide H_2N-Aib-L-AlaNHMe (60 mg, 0.312 mmol) and DIPEA (2 equiv., 0.044 mL, until pH 8) were added to the mixture. The reaction was stirred at 25 °C overnight (TLC: CH_2Cl_2/MeOH, 10:1). The mixture was washed with aqueous HCl (3N, 2 × 5 mL), H_2O (5 mL), and finally with $NaHCO_3$ (2 × 5 mL). The organic layer was dried over Na_2SO_4, and the solvent was evaporated under vacuum. The crude mixture was crystallized from CH_2Cl_2/Et_2O to afford crude peptide **10** (40 mg, 50%). A further purification was performed by HPLC (phase A: 95% H_2O, 5% CH_3CN, 1 mL TFA; phase B: 95% CH_3CN, 5% H_2O, 1 mL TFA; elution gradient: 95% A for 5 min, then 95−30% A in 20 min) to give peptide **10** (20 mg, 25%). During the purification, we observed the formation of a byproduct corresponding to bicyclic derivative **11**. Alternatively, pure peptide **10** (30 mg, 38%) can be obtained directly from the crude product by performing a second crystallization. Mp 120 °C (CH_2Cl_2/Et_2O); $[\alpha_D]^{25}$ +6.2 (c 0.2, MeOH); IR (KBr) ν_{max} 3400, 1740 cm^{-1}; ^1H NMR (CD_3CN, 300 MHz) δ 8.92 (s, 1H), 7.94 (d, J = 7.2, 2H), 7.69 (brs, 1H), 7.60 (d, J = 10.9, 1H), 7.54−7.51 (m, 3H), 7.45 (d, J = 3.9, 1H), 7.39−7.17 (m, 7H), 4.71 (brs, 1H), 4.26−4.08 (m, 1H), 3.93−3.87 (m, 1H), 3.70−3.31 (m, 4H), 3.13−3.03 (m, 1H), 2.83−2.71 (m, 2H), 2.66 (d, J = 4.6, 3H), 2.59−1.90 (m, 5H), 1.55−1.32 (m, 12H); ^{13}C NMR (CD_3CN, 75 MHz) δ 15.8, 16.9, 23.0, 25.3, 26.4, 28.5, 30.1, 31.5, 34.3, 36.5, 42.7, 49.7, 52.4, 56.6, 62.0, 65.5, 126.1, 127.8, 128.4, 128.6, 129.1, 129.5, 130.3, 132.0, 132.3, 133.7, 134.2, 139.0, 167.8, 168.5, 173.2, 174.1, 174.5, 175.5; MS (ESI+) 651.3 [M + 1]; $C_{34}H_{46}N_6O_7$ Calcd for C 62.75, H 7.12, N 12.91; found C 62.56, H 7.34, N 13.17.

Synthesis of 12. Alcohol **5a** (0.26 mmol) was dissolved in CH_2Cl_2 (3 mL) and 3-tritylsulfanyl propionic acid (100 mg, 0.286 mmol) was added. After cooling to 0 °C, DMAP (3 mg, 0.026 mmol) was added, and DCC (36 mg, 0.286 mmol) dissolved in CH_2Cl_2 (1 mL) was added dropwise to the solution. The reaction was stirred for 3h at 25 °C (TLC: CH_2Cl_2/AcOEt, 1:1), and then the mixture was washed with $NaHCO_3$ (5 mL) and H_2O (5 mL). The organic layer was dried over Na_2SO_4, and the solvent was evaporated under vacuum. Pure compound **12** (155 mg, 80%) was obtained after crystallization. Mp 80 °C (AcOEt/Et_2O); $[\alpha_D]^{25}$ −8.7 (c 0.2, MeOH); IR (KBr) ν_{max} 3326, 1738 cm^{-1}; ^1H NMR ($CDCl_3$, 200 MHz) δ 7.77−7.70 (m, 2H), 7.51−7.17 (m, 23H), 6.09 (bs, 1H), 5.01−4.76 (m, 1H), 4.74 (bs, 1 H), 4.39−4.01 (m, 2H), 3.69 (s, 3H), 3.39−3.21 (m, 3H), 2.94−2.84 (m, 2H), 2.59−2.45 (m, 2H), 2.02−1.45 (m, 6H); ^{13}C NMR ($CDCl_3$, 75 MHz) δ 24.5, 24.7, 25.5, 29.8, 33.3, 33.8, 35.3, 50.5, 52.8, 60.6, 64.3, 67.2, 126.9 (x4), 127.2 (x2), 127.4 (x2), 127.9, 128.1 (x4), 128.4,

DOI: 10.1021/acs.joc.5b00396
J. Org. Chem. 2015, 80, 5507−5516

128.7, 128.8, 129.1, 129.2, 129.5, 129.7, 129.8 (x4), 132.1, 134.0, 137.6, 144.7, 147.1, 157.8, 167.4, 171.7, 173.2, 174.9; MS (ESI+) 777.5 [M + 23]; $C_{46}H_{46}N_2O_6S$ Calcd for C 73.18, H 6.14, N 3.71; found C 72.91, H 6.35, N 3.65.

Preparation of Covered Gold Nanoparticles. In a typical experiment, **12** (0.5 mmol) and $HAuCl_4{\cdot}3H_2O$ (0.25 mmol) were combined in a 4:1 methanol/milli-Q water solvent mixture (10 mL). The resulting solution was stirred at 0 °C for 1 h. To this solution was rapidly added a cold $NaBH_4$ (2.5 mmol) solution in MeOH (2 mL), and the resulting mixture was stirred at room temperature for an additional 4 h. The reaction was quenched by the addition of 0.1 M HCl (1 mL). The solvent mixture was removed under reduced pressure to dryness, and the dark residue was dissolved in CH_2Cl_2 (20 mL), washed with H_2O, dried over anhydrous Na_2SO_4, and evaporated to dryness. Subsequently, the crude product was dissolved in MEOH, passed through a 20 μm microfilter, and afterward precipitated by adding a large amount of Et_2O. Finally, the corresponding AuNps were obtained after centrifugation.

Determination of AuNp-12 Conjugate Structural Information. The number of Au atoms in the relative AuNps were calculated from (a) the dimensions of the metallic core (diameter) observed in the TEM images, (b) the density of bulk metal (55 atoms/nm^3), and (c) applying the sphere model. The numbers of moieties conjugated to the inorganic clusters were calculated from the TGA weight losses (corresponding to the weight fractions of the organic coating monolayer on the inorganic cluster) and the molecular weight of the related oligomers conjugated to the inorganic core. Consequently, the oligomer footprints of the different AuNps were calculated by relating the number of oligomers linked on the gold surface with the dimensional information obtained by the TEM analysis.

■ ASSOCIATED CONTENT

Supporting Information

CIF file with X-ray data for **4a** and NMR data for compounds **4a**, **10**, and **11**; HPLC spectrum of pure compound **10**; ^{1}H, and ^{13}C NMR spectra for all new compounds; geometries of representative structures of peptide **10**; and Amber ff99SB library for Oxo-Azn **5a**. The Supporting Information is available free of charge on the ACS Publications website at DOI: 10.1021/acs.joc.5b00396.

■ AUTHOR INFORMATION

Corresponding Author

*E-mail: sara.pellegrino@unimi.it.

Notes

The authors declare no competing financial interest.

■ ACKNOWLEDGMENTS

Funding for this work was provided by MIUR (PRIN 2010-2011 Proj. 2010NRREPL).

■ REFERENCES

(1) (a) Alex, S.; Tiwari, A. *J. Nanosci. Nanotechnol.* **2015**, *15*, 1869−1894. (b) Yongsheng, M.; Pengxia, L.; Zhou, Y.; Dong, W.; Wanli, H.; Hui, C.; Huai, Y. *RSC Adv.* **2015**, *5*, 140−145. (c) Figuero, E. R.; Lina, A. Y.; Yana1, J.; Luoa, L.; Fosterb, A. E.; Drezek, R. A. *Biomaterials* **2014**, *35*, 1725−1734. (d) Sapsford, K. E.; Algar, W. R.; Berti, L.; Boeneman Gemmill, K.; Casey, B. J.; Oh, E.; Stewart, M. H.; Medintz, I. L. *Chem. Rev.* **2013**, *113*, 1904−2074. (e) Jadhav, S. A. *J. Mater. Chem.* **2012**, *22*, 5894. (f) Prats-Alfonso, E.; Albericio, F. *J. Mater. Sci.* **2011**, *46*, 7643−7648. (g) Giljohann, D. A.; Seferos, D. S.; Daniel, W. L.; Massich; Patel, P. C.; Mirkin, C. A. *Angew. Chem., Int. Ed.* **2010**, *49*, 3280−3294.

(2) (a) Osante, I.; Polo, E.; Revilla-López, G.; de la Fuente, J. M.; Alemán, C.; Cativiela, C.; Díaz, D. *J. Nanopart. Res.* **2014**, *16*, 2224−2236. (b) Srisombat, L.; Jamison, A. C.; Lee, T. R. *Colloid Surf., A* **2011**, *390*, 1−19.

(3) (a) Panda, J. J.; Chauhan, V. S. *Polym. Chem.* **2014**, *5*, 4418−4436. (b) Parween, S.; Misra, A.; Ramakumar, S.; Chauhan, V. S. *J. Mater. Chem. B* **2014**, *2*, 3096−3106. (c) Montenegro, A.; Ghadiri, V.; Granja, J. R. *Acc. Chem. Res.* **2013**, *46*, 2955−2965. (d) Hourani, R.; Zhang, C.; van der Weegen, R.; Changyi, L. R.; Keten, L. S.; Helms, B. A.; Xud, T. *J. Am. Chem. Soc.* **2011**, *133*, 15296−15299. (e) Lalatsa, A.; Schätzlein, A. G.; Mazza, M.; Hang Le, T. B.; Uchegbue, I. F. *J. Controlled Release* **2012**, *161*, 523−553.

(4) (a) Leea, E.-J.; Bea, C. L.; Vinsona, A. R.; Richesa, A. G.; Fehra, F.; Gardinera, J.; Gengenbacha, T. R.; Winklera, D. A.; Haylock, D. *Biomaterials* **2015**, *37*, 82−93. (b) de Bruyn Ouboter, D.; Schuster, T. B.; Sigg, S. J.; Meier, W. P. *Colloids Surf., B* **2013**, *112*, 542−547.

(5) Aili, D.; Gryko, P.; Sepulveda, B.; Dick, J. A. G.; Kirby, N.; Heenan, R.; Baltzer, L.; Liedberg, B.; O Mary, P. R.; Stevens, M. M. *Nano Lett.* **2011**, *11*, 5564−5573.

(6) (a) Parween, S.; Ali, A.; Chauhan, V. S. *ACS Appl. Mater. Interfaces* **2013**, *5*, 6484−6493. (b) Rio-Echevarria, I. M.; Tavano, R.; Causin, V.; Papini, E.; Mancin, F.; Moretto, A. *J. Am. Chem. Soc.* **2011**, *133*, 8−11. (c) Aili, D.; Stevens, M. M. *Chem. Soc. Rev.* **2010**, *39*, 3358−3370.

(7) Avan, I.; Hall, C. D.; Katritzky, A. R. *Chem. Soc. Rev.* **2014**, *43*, 3575−3594.

(8) (a) Maffucci, I.; Pellegrino, S.; Clayden, J.; Contini, A. *J. Phys. Chem. B* **2015**, *119*, 1350−1361. (b) Demizu, Y.; Doi, M.; Kurihara, M.; Okuda, H.; Nagano, M.; Suemune, H.; Tanaka, M. *Org. Biomol. Chem.* **2011**, *9*, 3303−3312. (c) Gatto, E.; Porchetta, A.; Stella, L.; Guryanov, I.; Formaggio, F.; Toniolo, C.; Kaptein, B.; Broxterman, Q. B.; Venanzi, M. *Chem. Biodiversity* **2008**, *5*, 1263−1278. (d) Tanaka, M. *Chem. Pharm. Bull.* **2007**, *55*, 349−358. (e) Toniolo, C.; Crisma, M.; Formaggio, F.; Peggion, C.; Broxterman, Q. B.; Kaptein, B. *Biopolymers* **2004**, *76*, 162−176.

(9) (a) Pellegrino, S.; Contini, A.; Gelmi, M. L.; Lo Presti, L.; Soave, R.; Erba, E. *J. Org. Chem.* **2014**, *79*, 3094−3102. (b) Bonetti, A.; Clerici, F.; Foschi, F.; Nava, D.; Pellegrino, S.; Penso, M.; Soave, R.; Gelmi, M. L *Eur. J. Org. Chem.* **2014**, 3203−3209. (c) Pellegrino, S.; Contini, A.; Clerici, F.; Gori, A.; Nava, D.; Gelmi, M. L. *Chem.—Eur. J.* **2012**, *18*, 8705−8715. (d) Penso, M.; Foschi, F.; Pellegrino, S.; Testa, A.; Gelmi, M. L. *J. Org. Chem.* **2012**, *77*, 3454−3461. (e) Gassa, F.; Contini, A.; Fontana, G.; Pellegrino, S.; Gelmi, M. L. *J. Org. Chem.* **2010**, *75*, 7099−7106. (f) Pellegrino, S.; Clerici, F.; Gelmi, M. L. *Tetrahedron* **2008**, *64*, 5657−5665. (g) Cabrele, C.; Clerici, F.; Gandolfi, R.; Gelmi, M. L.; Molinari, F.; Pellegrino, S. *Tetrahedron* **2006**, *62*, 3502−3508. (h) Ruffoni, A.; Contini, A.; Soave, R.; Lo Presti, L.; Esposto, I.; Maffucci, I.; Nava, D.; Pellegrino, S.; Gelmi, M. L.; Clerici, F. *RSC Adv.* **2015**, *5*, 32643−32656.

(10) (a) Ribelin, T.; Katz, C. E.; Withrow, D.; Smith, S.; Manukyan, A.; Day, V. W.; Neuenswander, B.; Poutsma, J. L.; Aubé, J. *Angew. Chem, Int. Ed* **2008**, *47*, 6233−6235. (b) Katz, C. E.; Ribelin, T.; Withrow, D.; Basseri, Y.; Manukyan, A. K.; Bermudez, A.; Nuera, C. G.; Day, V. W.; Powell, D. R.; Poutsma, J. L.; Aubé, J. *J. Org. Chem.* **2008**, *73*, 3318−3327. (c) Katz, C. E.; Aubé, J. *J. Am. Chem. Soc.* **2003**, *125*, 13948−13949. (d) Sahasrabudhe, K.; Gracias, V.; Furness, K.; Smith, B. T.; Katz, C. E.; Reddy, D. S.; Aubé, J. *J. Am. Chem. Soc.* **2003**, *125*, 7914−7922. (e) Gracias, V.; Frank, K. E.; Milligan, G. L.; Aubé, J. *Tetrahedron* **1997**, *53*, 16241−16252. (f) Gracias, V.; Milligan, G. L.; Aubé, J. *J. Am. Chem. Soc.* **1995**, *117*, 8047−8048.

(11) (a) Jung, G.; Bruckner, H.; Bosch, R.; Winter, V.; Schaal, H.; Strahle, J. *Liebigs Ann. Chem.* **1983**, *7*, 1096−1106. (b) Francis, A. K.; Iqbal, M.; Balaram, P.; Vijayan, M. *Biopolymers* **1983**, *22*, 1499−1505. (c) Leibfritz, D.; Brunne, R. M.; Weihrauch, T.; Stelten, J.; Stohrer, W.-D.; Haupt, E. T. K *Liebigs Ann. Chem.* **1989**, *13*, 1017−1027. (d) Schweitzer-Stenner, R.; Gonzales, W.; Bourne, G. T.; Feng, J. A.; Marshall, G. R. *J. Am. Chem. Soc.* **2007**, *129*, 13095−13109 and references cited therein. (e) Longo, E.; Moretto, A.; Formaggio, F.; Toniolo, C. *Chirality* **2011**, *23*, 756−760 and reference cited therein.

(12) (a) Nuñez-Villanueva, D.; Infantes, L.; García-Lopez, M. T.; González-Muñiz, R.; Martín-Martínez, M. *J. Org. Chem.* **2012**, *77*, 9833−9839. (b) Nuñez-Villanueva, D.; Infantes, L.; García-Lopez, M. T.; González-Muñiz, R. *J. Org. Chem.* **2011**, *76*, 6592−6603.

DOI: 10.1021/acs.joc.5b00396
J. Org. Chem. 2015, 80, 5507−5516

(13) An exception involved the terminal Ala4, which had a widened φ (averaged approximately −85 deg) and a positive average ψ, although characterized by a high standard deviation, potentially resulting in difficulty in the clusterization process due to higher conformational variability of the C-terminal region with respect to the remaining peptide.
(14) (a) Alvarez, M. M.; Khoury, J. T.; Schaaff, T. G.; Shafigullin, M. N.; Vezmar, I.; Whetten, R. L. *J. Phys. Chem. B* **1997**, *101*, 3706−3712. (b) Mie, G. *Ann. Phys.* **1908**, *25*, 377−445. (c) Kreibig, U.; Genzel, L. *Surf. Sci.* **1985**, *156*, 678−700. (d) Quinten, M.; Kreibig, U. *Surf. Sci.* **1986**, *172*, 557−577. (e) Barnett, R. N.; Cleveland, C. L.; Häkkinen, H.; Luedtke, W. D.; Yannouleas, C.; Landman, U. *Eur. Phys. J. D* **1999**, *9*, 95−104. (f) Kelly, K. L.; Coronado, E. L. L.; Schatz, G. C. *J. Phys. Chem. B* **2003**, *107*, 668−677.
(15) (a) Gautier, C.; Bürgi, T. *J. Am. Chem. Soc.* **2006**, *128*, 11079−11087. (b) Longo, E.; Orlandin, A.; Mancin, F.; Scrimin, P.; Moretto, A. *ACS Nano* **2013**, *11*, 9933−9939.
(16) Knoppe, S.; Dolamic, I.; Dass, A.; Bürgi, T. *Angew. Chem., Int. Ed.* **2012**, *51*, 7589−7591.
(17) *Molecular Operating Environment (MOE)*, 2013.08; Chemical Computing Group, Inc.: Montreal, Canada, 2013.
(18) Dupradeau, F.-Y.; Pigache, A.; Zaffran, T.; Savineau, C.; Lelong, R.; Grivel, N.; Lelong, D.; Rosanski, W.; Cieplak, P. *Phys. Chem. Chem. Phys.* **2010**, *12* (28), 7821−7839.
(19) Hornak, V.; Abel, R.; Okur, A.; Strockbine, B.; Roitberg, A.; Simmerling, C. *Proteins: Struct., Funct., Bioinf.* **2006**, *65* (3), 712−725.
(20) Case, D. A.; Babin, V.; Berryman, J. T.; Betz, R. M.; Cai, Q.; Cerutti, D. S.; Cheatham, T. E., III; Darden, T. A.; Duke, R. E.; Gohlke, H.; Goetz, A. W.; Gusarov, S.; Homeyer, N.; Janowski, P.; Kaus, J.; Kolossváry, I.; Kovalenko, A.; Lee, T. S.; LeGrand, S.; Luchko, T.; Luo, R.; Madej, B.; Merz, K. M.; Paesani, F.; Roe, D. R.; Roitberg, A.; Sagui, C.; Salomon-Ferrer, R.; Seabra, G.; Simmerling, C. L.; Smith, W.; Swails, J.; Walker, R. C.; Wang, J.; Wolf, R. M.; Wu, X.; Kollman, P. A. *AMBER 14*; University of California: San Francisco, CA, 2014.
(21) Onufriev, A.; Bashford, D.; Case, D. A. *Proteins: Struct., Funct., Bioinf.* **2004**, *55*, 383−394.
(22) Humphrey, W.; Dalke, A.; Schulten, K. *J. Mol. Graphics Modell.* **1996**, *14*, 33−38.
(23) Kabsch, W.; Sander, C. *Biopolymers* **1983**, *22*, 2577−2637.

DOI: 10.1021/acs.joc.5b00396
J. Org. Chem. 2015, 80, 5507−5516